

Constraining high energy interaction mechanisms by studying forward hadron production at the LHC

S. Ostapchenko^{1,2}, M. Bleicher^{1,3}, T. Pierog⁴ and K. Werner⁵

¹*Frankfurt Institute for Advanced Studies, 60438 Frankfurt am Main, Germany*

²*D.V. Skobeltsyn Institute of Nuclear Physics, Moscow State University, 119992 Moscow, Russia*

³*Institute for Theoretical Physics, Goethe-Universität, 60438 Frankfurt am Main, Germany*

⁴*Karlsruhe Institute of Technology, Institut für Kernphysik, Postfach 3640, 76021 Karlsruhe, Germany*

⁵*SUBATECH, University of Nantes-IN2P3/CNRS-EMN, 4 rue Alfred Kastler, 44307 Nantes Cedex 3, France*

July 30, 2018

Abstract

We demonstrate that underlying assumptions concerning the structure of constituent parton Fock states in hadrons make a strong impact on the predictions of hadronic interaction models for forward hadron spectra and for long-range correlations between central and forward hadron production. Our analysis shows that combined studies of proton-proton collisions at the Large Hadron Collider by central and forward-looking detectors have a rich potential for discriminating between the main model approaches.

1 Introduction

The modeling of high energy hadronic interactions is of considerable importance for experimental studies at the Large Hadron Collider (LHC) and, especially, in astroparticle physics. Working on event generators for hadronic and nuclear collisions, one generally aims at describing the largest possible part of the corresponding phase space using perturbative methods. Nevertheless, one can not restrain from using phenomenological approaches when dealing with essentially nonperturbative soft physics which unavoidably enters such developments. This applies, in particular, to the treatment of constituent parton Fock states in hadrons.

Considering, e.g., a proton-proton collision in the center of mass (c.m.) frame, we generally deal with multiple binary interactions of partons from two parton clouds formed prior to the collision. We are interested here in the momentum distribution of these multiparton states, which is related to the evolution of parton cascades in hadrons. The picture behind the corresponding treatment for the majority of current generators of hadronic collisions is shown schematically on the left-hand side (lhs) of Fig. 1. At large Feynman x , one usually starts from the same universal parton Fock state. Additional partons (sea quarks and gluons) giving rise to new branches of the parton cascade, which take part in the multiple scattering processes, result from the evolution of the parton density corresponding to this initial state and are typically distributed as $\propto 1/x$ in the very high energy limit. For example, the DIPSY generator [1] contains an explicit treatment of this kind, developed in the dipole framework. Such a picture reflects itself in the hadron production pattern predicted by the models: multiple scattering mostly affects central particle production, while having a weak influence on forward hadron spectra. Indeed, the latter are formed by the hadronization of partons emerging from the initial part of the underlying parton cascade, which starts from the same initial conditions and covers a short rapidity interval, being thus weakly dependent on further development of the cascade.

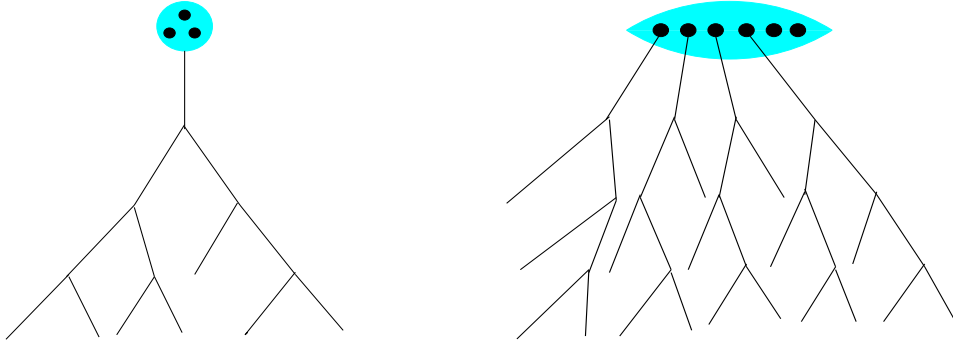


Figure 1: Schematic view on the initial part of the parton cascade in the proton. Left: the cascade starts from the same universal parton Fock state; new partons participating in multiple scattering processes emerge from the cascade development, being characterized by $\propto 1/x$ distributions for the light-cone momentum fraction. Right: the proton is represented by a superposition of Fock states consisting of different numbers of large x constituent partons; the more abundant multiple scattering the larger Fock states get involved in the process.

Alternatively, one may consider a proton to be represented by a superposition of a number of Fock states containing different numbers of large x constituent partons, as shown schematically on the right-hand side of Fig. 1. Further cascading of these partons “dresses” them with low x parton clouds. As the overall parton multiplicity in the central rapidity region is roughly proportional to the number of initial constituent partons, stronger multiple scattering is typically associated with larger Fock states. Thus, there is a strong long-range correlation between central and forward particle production; higher multiplicity in the central rapidity region reflects stronger multiple parton scattering. In turn, this implies that larger numbers of constituent partons are involved in the process, which has a strong impact on forward hadron spectra. This approach is typically used in models developed within the Reggeon field theory (RFT) framework [2], like EPOS [3, 4] or QGSJET-II [5, 6]. It is noteworthy that a similar picture arises when considering the incident proton to be at rest and using e.g. the color glass condensate framework: In the very high energy limit, there is a dense cloud of partons originating from the parton cascade in the target proton; these partons pass through the projectile proton and undergo multiple scattering off its valence constituents [7].

To quantify the discussion, let us consider the (quasi-)eikonal RFT approach [8], where the proton is represented by a superposition of Fock states consisting of different numbers n of constituent partons: $|p\rangle = \sum_n \sqrt{C_n} |n\rangle$, C_n being the respective partial weights. The behavior of the corresponding parton light-cone momentum fraction distributions $F^{(n)}(x_1, \dots, x_n)$ is described in the low x limit by secondary Reggeon asymptotics¹ [11]:

$$F^{(n)}(x_1, \dots, x_n) \Big|_{x_i \rightarrow 0} \propto x_i^{-\alpha_{\mathbb{R}}(0)}, \quad \alpha_{\mathbb{R}}(0) \simeq 0.5. \quad (1)$$

Thus, we deal with Fock states formed by predominantly large x constituent partons. The interaction is mediated by multi-Pomeron exchanges; the partial contribution of an exchange by m Pomerons rises with c.m. energy squared s like $\propto s^{m(\alpha_{\mathbb{P}}(0)-1)}$, where $\alpha_{\mathbb{P}}(0) > 1$ is the Pomeron intercept. Hence, the higher the energy the more abundant the multiple scattering and Fock states with increasing numbers of partons coming into play. Due to the so-called Abramovskii-Gribov-Kancheli (AGK) cancellations [12], multi-Pomeron configurations do not contribute to the inclusive

¹ We restrict our discussion to typical hadronic collisions that give rise to the bulk of secondary particle production. Hence, we neglect contributions of parton Fock states containing heavy quarks [9], which may generally be important for more dedicated observables (see Ref. [10] for a recent review).

hadron spectra in the central rapidity region and the latter rise as a power of energy like

$$\left. \frac{d\sigma_{pp}^h(s, y)}{dy} \right|_{y \rightarrow 0} \propto s^{\alpha_{\mathbb{P}}(0)-1}. \quad (2)$$

Moreover, taking into account the energy-momentum sharing between constituent partons at the amplitude level, the AGK cancellations apply to the whole kinematic space [13] and the complete hadron spectra are characterized by the powerlike behavior:²

$$\frac{E d^3\sigma_{pp}^h(s, p)}{dp^3} \propto s^{\alpha_{\mathbb{P}}(0)-1}. \quad (3)$$

In turn, inclusive hadron spectra for proton-nucleus collisions are related to the ones for pp interactions as

$$\frac{E d^3\sigma_{pA}^h(s, p)}{dp^3} = A \frac{E d^3\sigma_{pp}^h(s, p)}{dp^3}. \quad (4)$$

Such a picture gives rise to the strongest possible correlation between central and forward particle production: both originate from the hadronization of Pomeron “strings” stretched between the projectile and target (large x) constituent partons [14].

As discussed in Ref. [14], Eqs. (3) and (4) should fail at sufficiently high energies as the total light-cone momentum of produced hadrons would exceed the one of the incident proton in the limits of large s or large A . In the high energy limit, one has to take into consideration the contributions of so-called enhanced diagrams that describe Pomeron-Pomeron interactions [15]. This considerably suppresses the forward hadron spectra compared to Eqs. (3) and (4) and weakens the correlation between central and forward particle production [12, 14]. The corresponding treatment of the QGSJET-II model is based on an all-order resummation of the respective graphs [16] while the EPOS model employs an effective treatment of lowest order diagrams [3].

It is noteworthy that the alternative approach corresponding to the schematic picture in the lhs of Fig. 1 can be recovered here if one restricts oneself to the contributions of the enhanced diagrams only. To be more precise, one has to consider only those graphs where a single Pomeron is coupled to the projectile proton, respectively, to the target proton or to a target nucleon in case of pA collision. In the pp case, this leads to the set of the so-called Pomeron loop graphs. For proton-nucleus collisions, also the “fan” diagrams developing in the target direction have to be considered. This would lead precisely to the picture in the lhs of Fig. 1. While for central density of produced particles, Eq. (2) will remain approximately valid, forward hadron spectra will scale proportionally to the inelastic cross section: $d\sigma_{pp}^h/dx_{\mathbb{F}}|_{x_{\mathbb{F}} \rightarrow 1} \propto \sigma_{pp}^{\text{inel}}(s)$, $x_{\mathbb{F}}$ being the Feynman x variable. In other words, in the fragmentation region Feynman x scaling would hold with a good accuracy:

$$\frac{1}{\sigma_{pp}^{\text{inel}}(s)} \left. \frac{d\sigma_{pp}^h(s, x_{\mathbb{F}})}{dx_{\mathbb{F}}} \right|_{x_{\mathbb{F}} \rightarrow 1} \simeq f(x_{\mathbb{F}}). \quad (5)$$

In this paper, we analyze the differences between Monte Carlo generators for high energy hadronic collisions, which employ the two above-discussed approaches to the treatment of constituent parton Fock states in hadrons. In Section 2, we compare the energy dependence of forward hadron spectra in pp collisions, predicted by the EPOS-LHC [4] and QGSJET-II-04 [6] models, to the respective results of the alternative treatment corresponding to the picture in the lhs of Fig. 1, as implemented in the PYTHIA 6 (Perugia tune 350) [17, 18] and SIBYLL 2.3 [19] models. In Section 3, we illustrate how the two basic approaches can be discriminated by combined measurements of hadron production at the LHC by central and forward-looking detectors. Finally, we conclude in Section 5.

²In Eq. (3), we do not include the contribution to secondary hadron production from the hadronization of proton “remnants” formed by spectator partons [14].

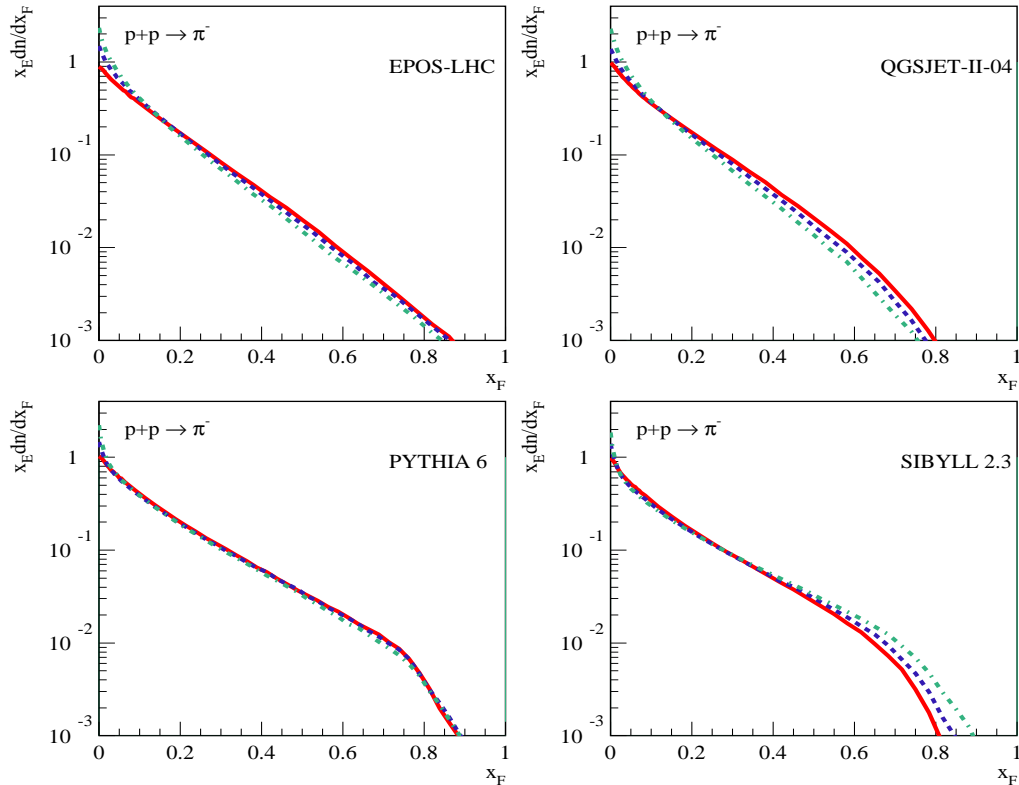


Figure 2: Feynman x spectra of negative pions in pp collisions at $\sqrt{s} = 10^2$ (solid), 10^3 (dashed), and 10^4 (dash-dotted) GeV, as calculated using EPOS-LHC (top left), QGSJET-II-04 (top right), PYTHIA 6 (bottom left), and SIBYLL 2.3 (bottom right).

2 Energy dependence of forward hadron spectra and of the “inelasticity”

An accurate model description of forward hadron production is of utmost importance for various experimental activities in the collider and astroparticle physics fields. It is relevant, for example, for studies of the inelastic diffraction at the LHC (see, e.g., the discussion in Ref. [20]) or to various astrophysical studies with charged cosmic rays and gamma rays, including indirect searches for dark matter, as discussed, e.g., in Refs. [21, 22, 23]. But of most crucial importance is the modeling of forward production for the interpretation of experimental data on ultrahigh energy cosmic rays which are studied with the extensive air shower (EAS) techniques – measuring the properties of nuclear-electromagnetic cascades induced by primary cosmic ray particles (protons or nuclei) in the atmosphere. Indeed, the energy dependence of forward hadron spectra impacts strongly the relation between the properties of the primary particles and the calculated EAS characteristics, in particular, for the so-called EAS maximum position X_{\max} – the depth in the atmosphere where the maximal number of ionizing particles is observed [24, 25]. As discussed in Ref. [24], the calculated X_{\max} is especially sensitive to model predictions for the so-called inelasticity – the relative energy loss of leading nucleons in proton-air collisions.

The differences in the predicted energy dependence of forward hadron spectra are illustrated in Fig. 2. There we plot Feynman x spectra of negative pions $x_E dn_{pp}^{\pi^-}/dx_F$ ($x_E = 2E/\sqrt{s}$) for pp collisions at $\sqrt{s} = 10^2$, 10^3 , and 10^4 GeV, as calculated with EPOS-LHC, QGSJET-II-04, PYTHIA 6, and SIBYLL 2.3. While all the models predict a similar energy rise of the pion yield in the central region ($x_F \simeq 0$), their results for the forward spectra differ considerably. For

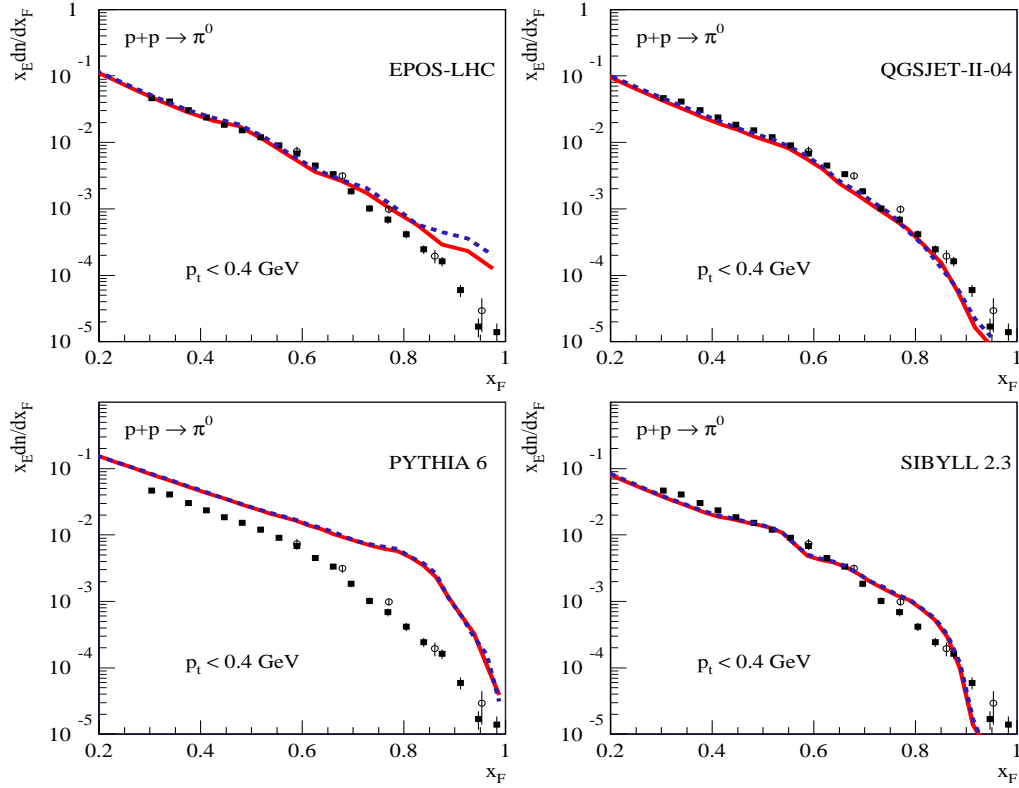


Figure 3: Feynman x spectra of neutral pions (for transverse momentum $p_t < 0.4$ GeV) in pp collisions at $\sqrt{s} = 7$ (solid) and 2.76 (dashed) TeV, as calculated using EPOS-LHC (top left), QGSJET-II-04 (top right), PYTHIA 6 (bottom left), and SIBYLL 2.3 (bottom right), compared to LHCf data [26] ($\sqrt{s} = 7$ TeV – filled squares, $\sqrt{s} = 2.76$ TeV – open circles).

PYTHIA 6, the Feynman x scaling of Eq. (5) holds to a very good accuracy: the spectral shape is practically independent of \sqrt{s} for $x_F \gtrsim 0.01$. SIBYLL 2.3 shows a similar behavior up to large x_F values; for $x_F \gtrsim 0.5$, it predicts a hardening of the very forward pion spectra, which is related to a specific treatment of the hadronization of the proton “remnant” state in that model. In contrast, for EPOS-LHC and QGSJET-II-04 the predicted energy dependence is rather different. For $x_F \lesssim 0.1$, the spectra rise with \sqrt{s} , though with increasing x_F this rise is strongly suppressed by absorptive effects, compared to the AGK-like dependence of Eq. (3). The suppression is especially strong in the very forward direction where we observe a significant “softening” of the predicted spectra. Comparing in Fig. 3 the model predictions for forward π^0 spectra at $\sqrt{s} = 2.76$ and 7 TeV with the respective measurements of the LHCf experiment [26], we observe a generally better agreement with the data for EPOS-LHC and QGSJET-II-04. However, the relatively small difference between the two collision energies does not allow one to make definite conclusions concerning the degree of the scaling violation.

In Fig. 4, we show the energy dependence of the inelasticity K_{pp}^{inel} of leading nucleons in pp collisions, predicted by the different models. The purely AGK-like behavior corresponding to Eq. (3) would give rise to a powerlike increase of the inelasticity: $K_{pp}^{\text{inel}}(s) \propto s^{\alpha_{\mathbb{P}}(0)-1}$. In reality, important contributions to forward nucleon spectra come from the hadronization of hadronic “remnant” states formed by spectator partons and from the inelastic diffraction, which should modify the s -dependence as

$$K_{pp}^{\text{inel}}(s) \simeq K_0 + \text{const} \times s^{\alpha_{\mathbb{P}}(0)-1}. \quad (6)$$

In the very high energy limit, such a rise should be necessarily damped by absorptive corrections,

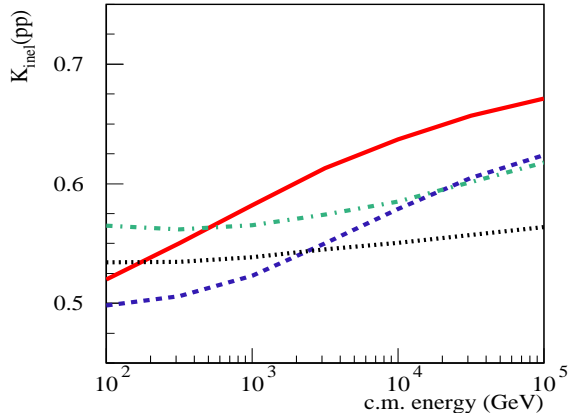


Figure 4: Energy dependence of the inelasticity of leading nucleons in pp collisions, as calculated using EPOS-LHC (solid), QGSJET-II-04 (dashed), PYTHIA 6 (dash-dotted), and SIBYLL 2.3 (dotted).

to prevent the violation of the energy conservation [14]. In Fig. 4, we observe indeed a substantial increase of the inelasticity predicted by EPOS-LHC and QGSJET-II-04. For the latter model, at $\sqrt{s} \simeq 10^2 - 10^4$ GeV K_{pp}^{inel} manifests the energy dependence described by Eq. (6), while for EPOS-LHC the stronger absorptive corrections damp it to just a logarithmic energy rise in this energy range. In turn, the mechanism corresponding to the schematic picture in the lhs of Fig. 1 should result in a rather weak energy dependence of the inelasticity, which we observe indeed in Fig. 4 for the PYTHIA 6 and SIBYLL 2.3 models.

3 How to discriminate between the interaction mechanisms?

Recent combined measurements by the CMS and TOTEM experiments of the pseudorapidity η density $dn_{pp}^{\text{ch}}/d\eta$ of produced charged hadrons in pp collisions [27] proved to be quite sensitive to the discussed interaction mechanisms. This is illustrated in Fig. 5 (left), where we compare the calculated $dn_{pp}^{\text{ch}}/d\eta$ for the different models to the CMS and TOTEM data, for the nondiffractive (ND) event selection adopted in the experimental analysis: at least one charged hadron produced both at $-6.5 < \eta < -5.3$ and at $5.3 < \eta < 6.5$. In the EPOS-LHC and QGSJET-II-04 models, the predicted $dn_{pp}^{\text{ch}}/d\eta$ is characterized by a relatively flat η -dependence, extending to large η values, in agreement with the experimental observations. In contrast, for the other two models the η -density of produced hadrons quickly falls down in the forward direction, reflecting the quick decrease of the number of constituent partons when parton momentum fraction increases.

It is noteworthy that the adopted experimental selection complicates somewhat the model comparison – as the fraction of ND events which satisfy the trigger depends noticeably on the predicted absolute values of $dn_{pp}^{\text{ch}}/d\eta$ at large η . Indeed, the probability for producing a rapidity gap of the rather small size $\Delta\eta \simeq 1$ by fluctuations in ND events is rather high [28, 29] and varies strongly from model to model (see Ref. [30] for a detailed quantitative study). Thus, a cleaner comparison may be provided by a central detector trigger, e.g. requesting at least one charged hadron of $p_t > 0.1$ GeV to be detected at $|\eta| < 2.5$. The corresponding results plotted in Fig. 5 (right) show a good agreement between all the models in the central η region, which reflects the model calibration to the data of Run 1 of the LHC. On the other hand, the models diverge considerably in the forward η region, which reflects the above-discussed differences concerning the assumed structure of constituent parton Fock states: The results of EPOS-LHC and QGSJET-II-04 practically coincide with each other and are both substantially flatter compared to $dn_{pp}^{\text{ch}}/d\eta$ predicted by the other two models.

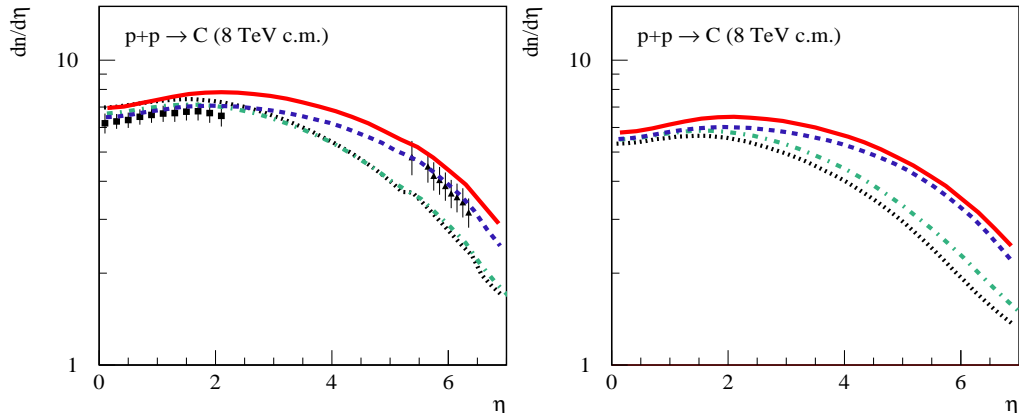


Figure 5: Pseudorapidity density of produced charged hadrons in pp collisions at $\sqrt{s} = 8$ TeV, as calculated using EPOS-LHC (solid), QGSJET-II-04 (dashed), PYTHIA 6 (dash-dotted), and SIBYLL 2.3 (dotted) for two different event selections: at least one charged hadron produced both at $-6.5 < \eta < -5.3$ and at $5.3 < \eta < 6.5$ (left panel) or at least one charged hadron of $p_t > 0.1$ GeV, produced at $|\eta| < 2.5$ (right panel). The data of the CMS and TOTEM experiments are shown by filled squares and filled triangles respectively.

As follows from the discussion in Section 1, a better way to discriminate between the two approaches for the treatment of constituent parton Fock states is via combined measurements of particle production by central and forward-looking detectors, triggering different levels of hadronic activity in the former. This is illustrated in Figs. 6 and 7 for pp collisions at $\sqrt{s} = 8$ and 13 TeV, where the predictions of the different models for $dn_{pp}^{\text{ch}}/d\eta$ are compared to each other for different event triggers: requesting at least 1, 5, 10, or 20 charged hadrons of $p_t > 0.1$ GeV to be detected at $|\eta| < 2.5$. While all the considered models agree approximately with each other in the central rapidity region, the results of the models diverge considerably at large η . In PYTHIA 6 and SIBYLL 2.3, enhancing the trigger conditions gives rise to the increasing density of produced hadrons at small η while leaving $dn_{pp}^{\text{ch}}/d\eta$ practically unchanged in the large η range. This is related to the fact that multiple scattering affects mostly the central particle production in the two models, while having a weak influence on forward hadron spectra. In contrast, in EPOS-LHC and QGSJET-II-04 also the forward η -density of produced hadrons is substantially enhanced, reflecting the strong correlations between central and forward hadron production in the two models: A stronger central activity implies an increasing role of proton Fock states containing numerous large x constituent partons.

The differences between the two basic approaches are best seen in the correlations of the signal strength in central and forward-looking detectors, which may be studied by the CMS and TOTEM experiments. This is illustrated in Fig. 8, where we plot for $\sqrt{s} = 8$ and 13 TeV the η -density of charged hadrons $dn_{pp}^{\text{ch}}/d\eta$ (for arbitrary transverse momenta) at $|\eta| = 6$ (averaged over the interval $5.5 < |\eta| < 6.5$) as a function of the central pseudorapidity density of charged hadrons of $p_t > 0.1$ GeV (averaged over the interval $|\eta| < 1$). Both EPOS-LHC and QGSJET-II-04 predict a strong correlation of the signal strength in CMS and TOTEM. The respective results of the two models practically coincide with each other, apart from the region corresponding to the tails of the multiplicity distributions. In contrast, for PYTHIA 6 and SIBYLL 2.3 such a correlation turns out to be twice weaker, being thus a clear experimental signature for discrimination between the two theoretical approaches depicted schematically in Fig. 1.

Another way for the model discrimination may be provided by measurements of very forward particle production, e.g. by the LHCf experiment, when supplemented by triggering different hadronic activities in the central detectors of ATLAS. This is illustrated in Figs. 9 and 10, where

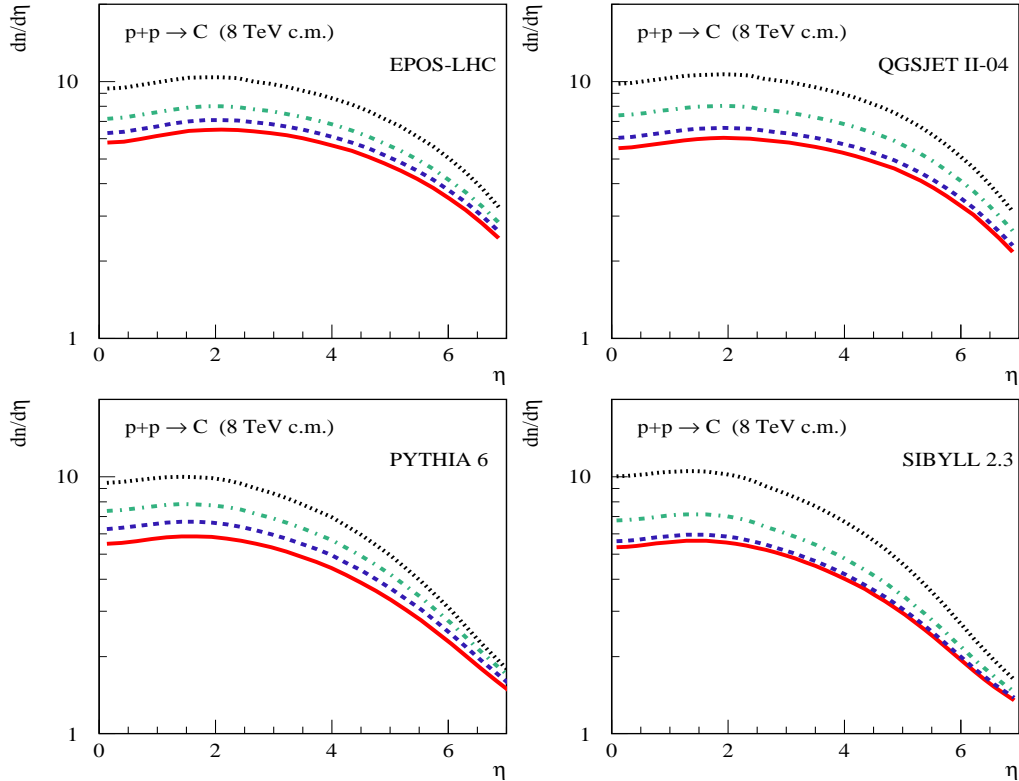


Figure 6: Pseudorapidity density of produced charged hadrons in pp collisions at $\sqrt{s} = 8$ TeV for different event selections: at least 1 (solid), 5 (dashed), 10 (dash-dotted), or 20 (dotted) charged hadrons of $p_t > 0.1$ GeV, produced at $|\eta| < 2.5$. Top left panel – EPOS-LHC, top right panel – QGSJET-II-04, bottom left panel – PYTHIA 6, bottom right panel – SIBYLL 2.3.

forward spectra of neutral pions in pp collisions at $\sqrt{s} = 8$ and 13 TeV are shown for a number of ATLAS triggers, calculated using the different interaction models. It is easy to see that SIBYLL and PYTHIA predict an almost perfect limiting fragmentation: For all the triggers considered, the spectral shapes remain practically identical at large Feynman x , the spectra being just rescaled downwards according to the corresponding event rates. This is a direct consequence of the decoupling of central and forward production in the two models: triggering more hadronic activity in the central detectors of ATLAS enhances the central production while having almost no impact on the forward hadron spectra. The picture changes drastically in the case of the EPOS-LHC and QGSJET-II-04 models characterized by strong long-range correlations between central and forward hadron production. Events with higher multiplicity in ATLAS, corresponding to enhanced multiple scattering, are dominated by contributions of Fock states with larger numbers of large x constituent partons. The energy-momentum sharing between these partons leaves its imprint on the very forward spectra of π^0 , which become noticeably softer, compared to the case of low multiplicity events.

An even more drastic consequence of the energy-momentum sharing between large x constituent partons is the considerable softening of forward nucleon spectra. Higher rates of multiple scattering, corresponding to enhanced hadronic activity in ATLAS, require larger numbers of constituent partons to be involved in particle production. Hence, smaller fractions of the initial proton momentum are left for spectator partons which finally form the “leading” (most energetic) nucleons. This effect is clearly seen in the predictions of EPOS-LHC and QGSJET-II-04 for the forward spectra of neutrons in pp collisions at $\sqrt{s} = 8$ and 13 TeV, as shown in Figs. 11 and 12 for the

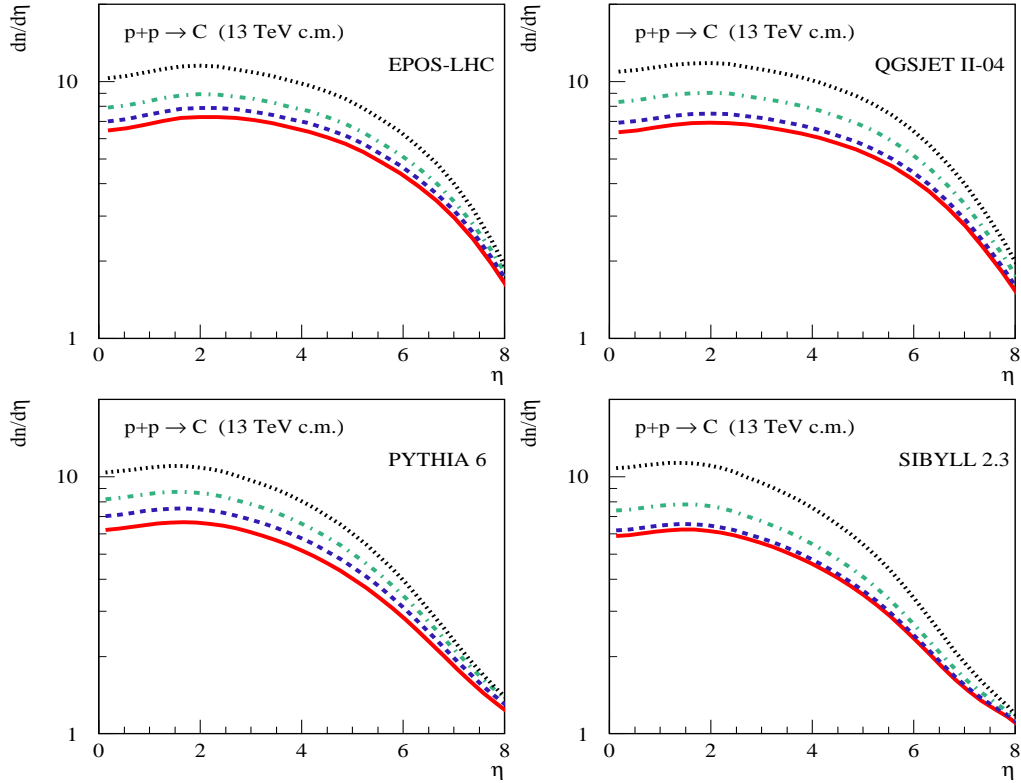


Figure 7: Same as in Fig. 6 for pp collisions at $\sqrt{s} = 13$ TeV.

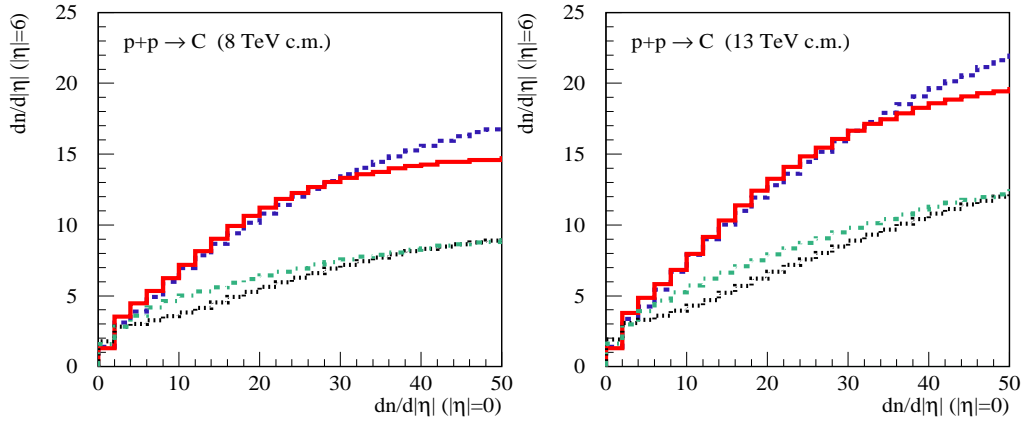


Figure 8: Pseudorapidity density of produced charged hadrons $dn_{pp}^{\text{ch}}/d|\eta|$ at $|\eta| = 6$ ($p_t > 0$) as a function of $dn_{pp}^{\text{ch}}/d|\eta|$ at $|\eta| = 0$ ($p_t > 0.1$ GeV) in pp collisions at $\sqrt{s} = 8$ TeV (left) and $\sqrt{s} = 13$ TeV (right), as calculated using EPOS-LHC (solid), QGSJET-II-04 (dashed), PYTHIA 6 (dash-dotted), and SIBYLL 2.3 (dotted).

pseudorapidity range covered by the LHCf experiment and for the same selection of ATLAS triggers as above. On the contrary, the shapes of forward neutron spectra predicted by SIBYLL and PYTHIA demonstrate much weaker sensitivity to varying the trigger conditions, as one may see in Figs. 11 and 12. This is because the additional constituent partons involved in multiple scattering are the low x ones. Hence, they typically pick up small fractions of the initial proton momenta,

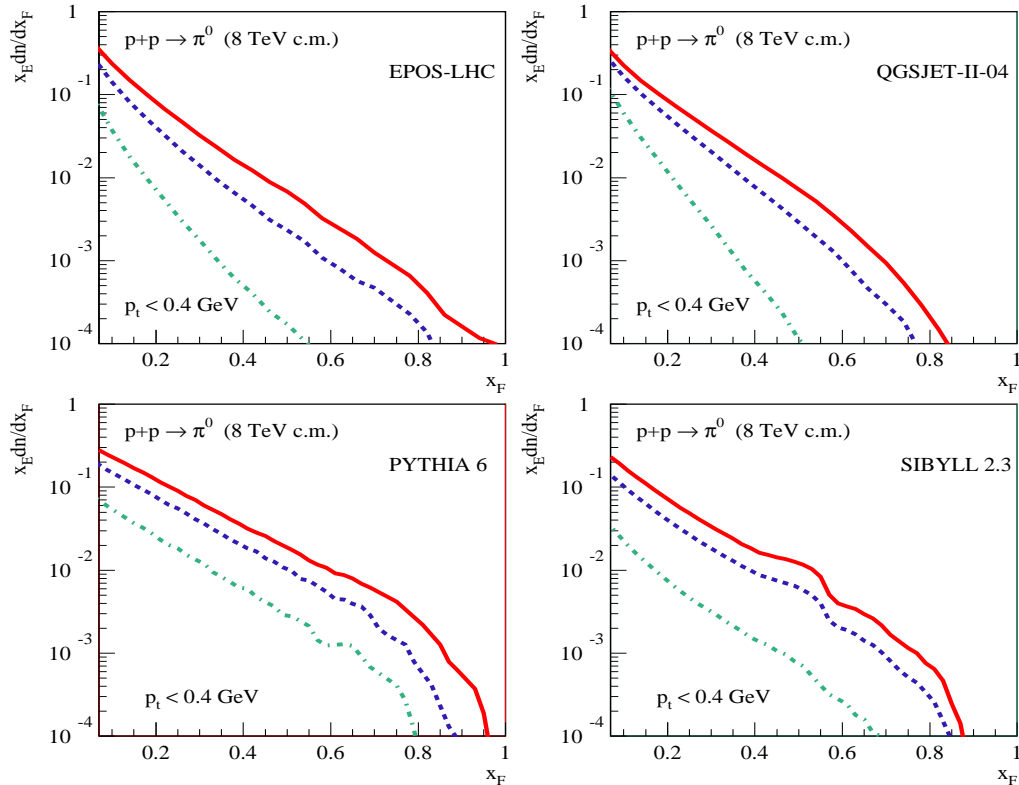


Figure 9: Feynman x spectra of neutral pions ($p_t < 0.4$ GeV) in pp collisions at $\sqrt{s} = 8$ TeV for different event selections: at least 1 (solid), 6 (dashed), or 20 (dash-dotted) charged hadrons of $p_t > 0.5$ GeV, produced at $|\eta| < 2.5$. Top left panel – EPOS-LHC, top right panel – QGSJET-II-04, bottom left panel – PYTHIA 6, bottom right panel – SIBYLL 2.3.

thus having a weak impact on the formation of leading nucleons.

4 Discussion

One may ask here natural questions about whether the above-discussed observables are robust enough with respect to a retuning of model parameters and how sensitive they are to other features of the interaction treatment. We may get some feeling about this by comparing in Figs. 13–15 the results of SIBYLL 2.3 and the pre-LHC version of the model (SIBYLL 2.1 [31]) for pp collisions at $\sqrt{s} = 8$ TeV for the ND η -density of charged particles, for the correlation of $dn_{pp}^{\text{ch}}/d|\eta|$ at $|\eta| = 6$ and $\eta = 0$, and for forward spectra of neutral pions as a function of particle activity in the central detector of ATLAS. As we can see from the figures, both the η -dependence in Fig. 13 and the x_F spectral shapes for particular ATLAS triggers in Fig. 15 demonstrate a noticeable dependence on the tuning. Nevertheless, both model versions predict a similarly weak correlation between the η -densities of produced charged hadrons at small and large η , as shown in Fig. 14. Similarly, both tunes demonstrate an almost perfect limiting fragmentation: The shape of the forward x_F -spectrum of produced neutral pions in Fig. 15 remains remarkably insensitive to the triggered particle activity in the ATLAS detector.

Similar conclusions follow from comparing the results of EPOS-LHC and QGSJET-II-04 with each other. Due to the large differences between the model approaches concerning the treatment of nonlinear interaction effects and due to the collective effects implemented in the hadronization procedure of the EPOS model, their predictions both for the inelasticity K_{pp}^{inel} in Fig. 4 and for the

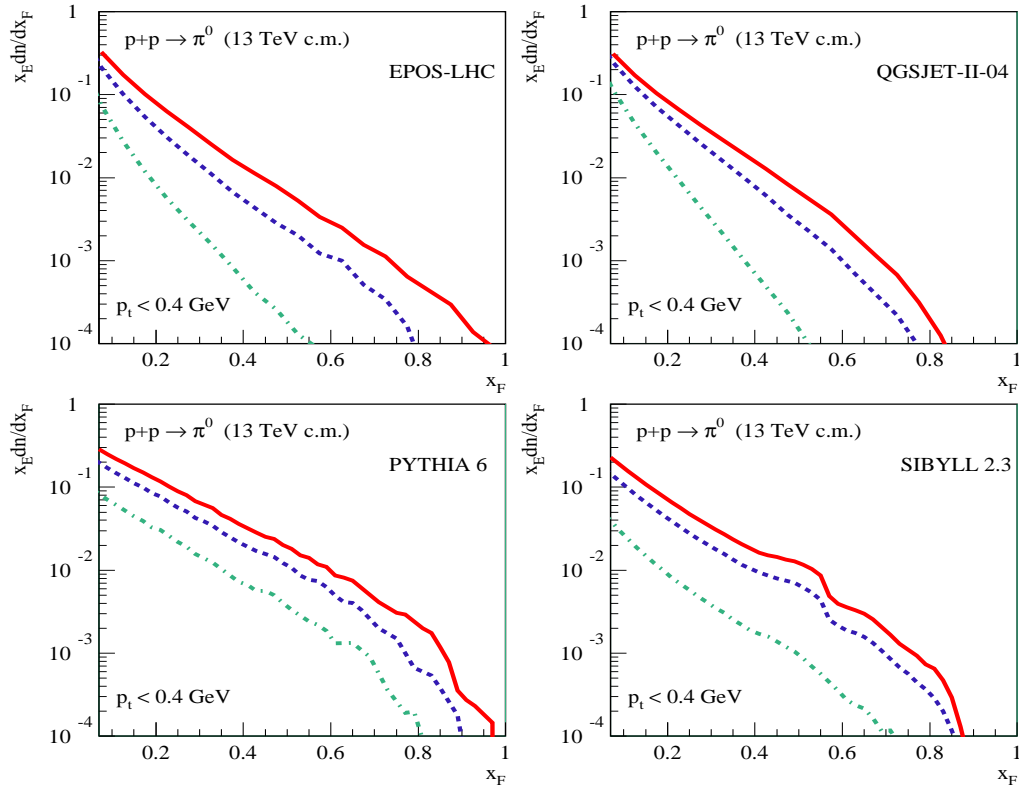


Figure 10: Same as in Fig. 9 for pp collisions at $\sqrt{s} = 13$ TeV.

forward spectra of π^0 s and neutrons in Figs. 9–12 differ considerably. Nevertheless, both models predict a similarly strong correlation between the strengths of particle production in the central and fragmentation regions (see Fig. 8) and a strong violation of the limiting fragmentation for very forward hadron production – both being the consequences of the similar model assumptions concerning the structure of constituent parton Fock states, discussed in Section 1.

Let us finally discuss the question of whether the differences between, e.g., PYTHIA 6 and SIBYLL 2.3 for the proposed observables give us the characteristic scale for the Monte Carlo tuning dependence of the presented results. In a sense, this is indeed the case – as these models represent the two extreme approaches corresponding to the mechanism of Fig. 1 (left). Indeed, in the SIBYLL model all multiple scattering processes except the first one are treated as binary gluon-gluon collisions, the initial state radiation (ISR) of partons being neglected. Hence, the decoupling between the central and forward particle production is maximal in that model. On the other hand, ISR in PYTHIA is traced backwards *for each hard scattering process independently*, down to the transverse momentum cutoff $p_t^{\text{cut}} \sim \text{few GeV}$. At first sight, one would tend to classify that model as corresponding to the picture in Fig. 1 (right). However, because the ISR in PYTHIA is matched to the parton distribution functions (PDFs) of gluons and sea quarks at the relatively high p_t^{cut} scale, the model corresponds effectively to the mechanism of Fig. 1 (left): Due to the steep low x rise of the respective PDFs and their strong suppression at $x \rightarrow 1$, the light-cone momenta of end-point partons in the backward cascades are sampled predominantly as $\propto 1/x$.

In relation to the latter, it is worth mentioning the recently developed Monash tune of the PYTHIA 8 generator [32], whose results agree well with the above-discussed data of CMS and TOTEM on $dn_{pp}^{\text{ch}}/d\eta$ and are generally similar to the ones of EPOS-LHC for forward hadron production in the kinematic range studied by the CMS experiment [33]. Among other improvements, the Monash tune employs the new NNPDF2.3LO PDF set [34] characterized by a rather hard

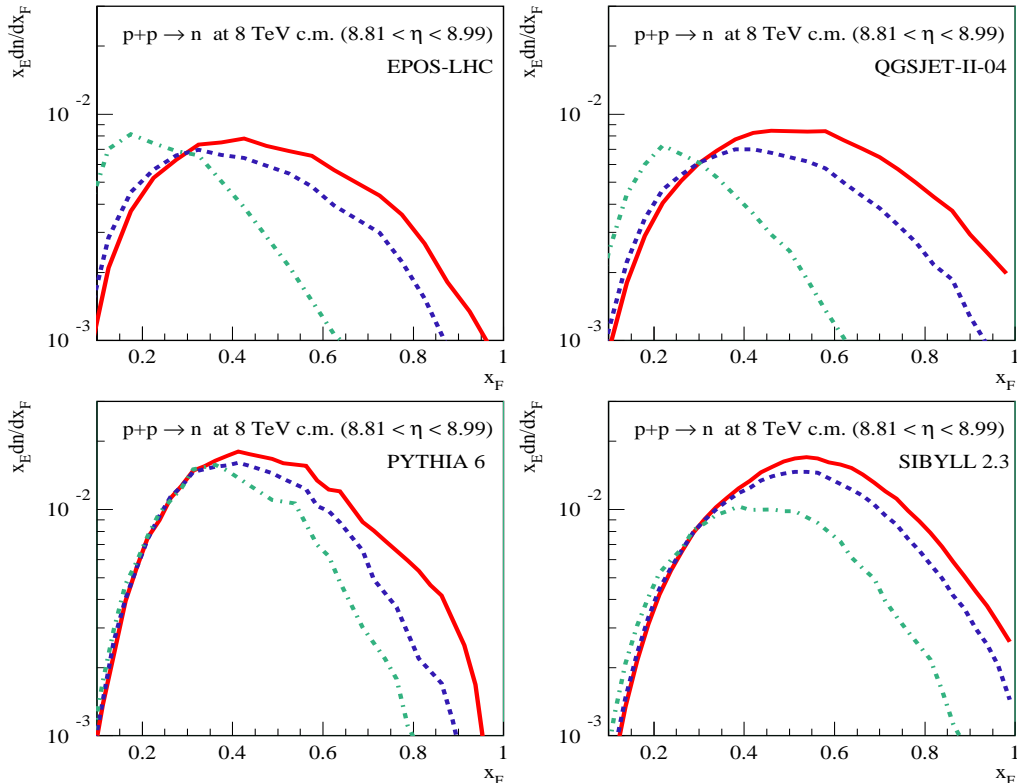


Figure 11: Feynman x spectra of neutrons ($8.81 < \eta < 8.99$) in pp collisions at $\sqrt{s} = 8$ TeV for different event selections: at least 1 (solid), 6 (dashed), or 20 (dash-dotted) charged hadrons of $p_t > 0.5$ GeV, produced at $|\eta| < 2.5$. The spectra for the latter two selections, plotted by dashed and dash-dotted lines, are rescaled to intersect the solid lines at $x_F = 0.3$. Top left panel – EPOS-LHC, top right panel – QGSJET-II-04, bottom left panel – PYTHIA 6, bottom right panel – SIBYLL 2.3.

gluon PDF. We believe it is the latter choice which governs the new model predictions for forward hadron production: Due to the presence of the “valencelike” contribution in the gluon PDF, initial state parton cascades for different multiple scattering processes end up with somewhat harder (i.e. having larger momentum fraction x) gluons and the model moves closer to the picture in Fig. 1 (right).³ Thus, a comparison of results of different tunes of PYTHIA 8, using different PDF sets, for the above-proposed observables is of interest.

5 Conclusions

One of the most crucial differences between current Monte Carlo generators of high energy hadronic collisions is related to the underlying assumptions concerning the structure of constituent parton Fock states in hadrons. These dominate the differences in model predictions concerning the energy dependence and target mass dependence of forward hadron production in hadron-proton and hadron-nucleus collisions. In close relation to that, these model differences have a crucial impact on the present theoretical uncertainties for basic characteristics of cosmic ray-induced extensive air showers, and hence also on the prospects of further success of studies of the primary composition of ultrahigh energy cosmic rays. We demonstrated that the different model approaches can be dis-

³Of importance here is not only that the hard gluon PDF is chosen but that it is applied to sample light-cone momenta for end-point gluons *in all the multiple initial state parton cascades*.

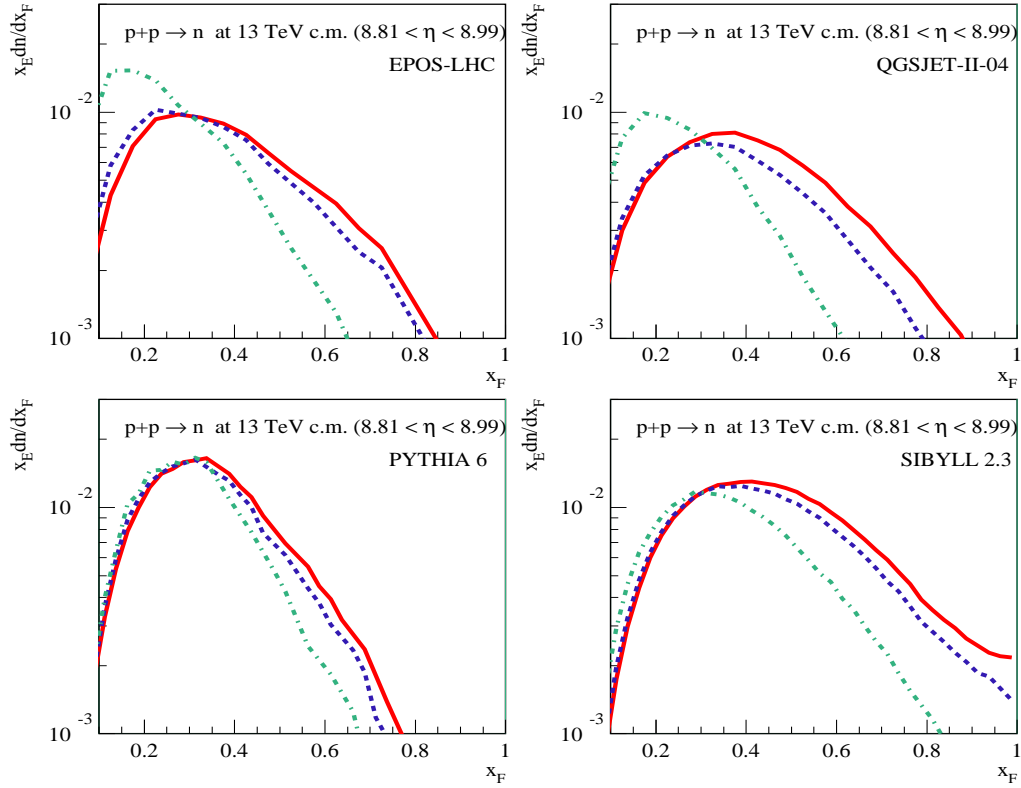


Figure 12: Same as in Fig. 11 for pp collisions at $\sqrt{s} = 13$ TeV.

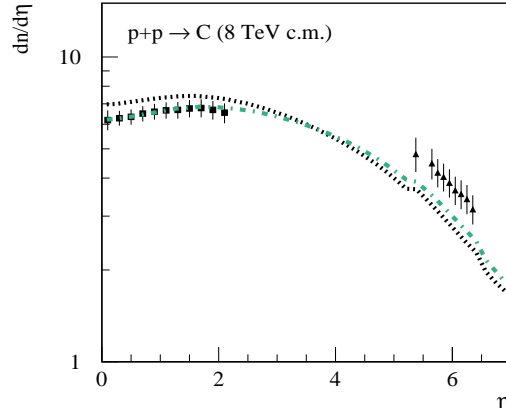


Figure 13: Same as in Fig. 5 (left) for the SIBYLL 2.3 (dotted) and SIBYLL 2.1 (dash-dotted) models.

criminated by measuring long-range correlations between central and forward hadron production. In particular, our analysis shows that combined studies of proton-proton collisions at the LHC by central and forward-looking particle detectors have a rich potential for such a discrimination. It is worth stressing that such studies do not generally require new measurements at the LHC – as the corresponding analysis can be performed using the already recorded experimental information from the common data-taking by CMS and TOTEM or, respectively, by ATLAS and LHCf.

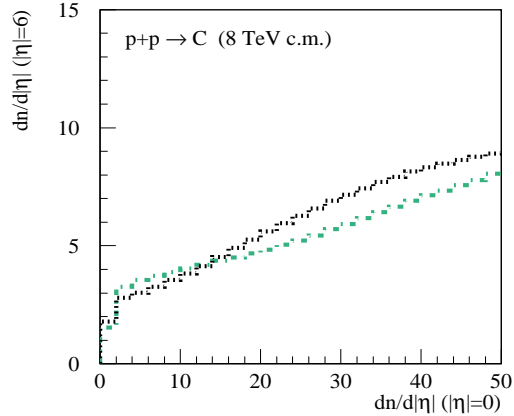


Figure 14: Same as in Fig. 8 (left) for the SIBYLL 2.3 (dotted) and SIBYLL 2.1 (dash-dotted) models.

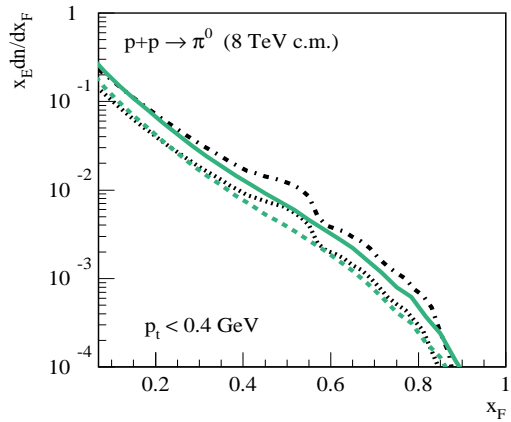


Figure 15: Feynman x spectra of neutral pions ($p_t < 0.4$ GeV) in pp collisions at $\sqrt{s} = 8$ TeV, as calculated using the SIBYLL 2.3 and SIBYLL 2.1 models for different event selections: at least 1 (solid – SIBYLL 2.1, dash-dotted – SIBYLL 2.3) or 6 (dashed – SIBYLL 2.1, dotted – SIBYLL 2.3) charged hadrons of $p_t > 0.5$ GeV, produced at $|\eta| < 2.5$.

Acknowledgments

This work was supported in part by Deutsche Forschungsgemeinschaft (Grant No. OS 481/1) and the State of Hesse via the LOEWE-Center HIC for FAIR.

References

- [1] E. Avsar, G. Gustafson, and L. Lönnblad, J. High Energy Phys. **07** (2005) 062; C. Flensburg, G. Gustafson, and L. Lönnblad, *ibid.* **08** (2011) 103.
- [2] V. N. Gribov, Sov. Phys. JETP **26**, 414 (1968).
- [3] K. Werner, F.-M. Liu and T. Pierog, Phys. Rev. C **74**, 044902 (2006).
- [4] T. Pierog, Iu. Karpenko, J. M. Katzy, E. Yatsenko, and K. Werner, Phys. Rev. C **92**, 034906 (2015).

- [5] S. Ostapchenko, Phys. Rev. D **74**, 014026 (2006).
- [6] S. Ostapchenko, Phys. Rev. D **83**, 014018 (2011).
- [7] H. J. Drescher, A. Dumitru, and M. Strikman, Phys. Rev. Lett. **94**, 231801 (2005);
H. J. Drescher and M. Strikman, *ibid.* **100**, 152002 (2008).
- [8] A. B. Kaidalov and K. A. Ter-Martirosyan, Phys. Lett. **117B**, 247 (1982).
- [9] S. J. Brodsky, C. Peterson and N. Sakai, Phys. Rev. D **23**, 2745 (1981); S. J. Brodsky, P. Hoyer,
C. Peterson and N. Sakai, Phys. Lett. **93B**, 451 (1980).
- [10] S. J. Brodsky *et al.*, Adv. High Energy Phys. **2015**, 231547 (2015).
- [11] A. B. Kaidalov, Sov. J. Nucl. Phys. **45**, 902 (1987).
- [12] V. A. Abramovskii, V. N. Gribov and O. V. Kancheli, Sov. J. Nucl. Phys. **18**, 308 (1974).
- [13] M. Hladik, H. J. Drescher, S. Ostapchenko, T. Pierog, and K. Werner, Phys. Rev. Lett. **86**,
3506 (2001).
- [14] H. J. Drescher, M. Hladik, S. Ostapchenko, T. Pierog, and K. Werner, Phys. Rep. **350**, 93
(2001).
- [15] O. V. Kancheli, JETP Lett. **18**, 274 (1973); J. L. Cardi, Nucl. Phys. **B75**, 413 (1974);
A. B. Kaidalov, L. A. Ponomarev and K. A. Ter-Martirosyan, Sov. J. Nucl. Phys. **44**, 468
(1986).
- [16] S. Ostapchenko, Phys. Lett. B **636**, 40 (2006); S. Ostapchenko, Phys. Rev. D **77**, 034009
(2008).
- [17] T. Sjöstrand, S. Mrenna and P. Z. Skands, J. High Energy Phys. **05** (2006) 026.
- [18] P. Z. Skands, Phys. Rev. D **82**, 074018 (2010).
- [19] F. Riehn, R. Engel, A. Fedynitch, T. K. Gaisser, and T. Stanev, Proc. Sci., ICRC2015 (2015),
558 [arXiv:1510.00568].
- [20] S. Ostapchenko, Phys. Lett. B **703**, 588 (2011).
- [21] T. Kamae, T. Abe, and T. Koi, Astrophys. J. **620**, 244 (2005).
- [22] M. Kachelriess and S. Ostapchenko, Phys. Rev. D **86**, 043004 (2012).
- [23] M. Kachelriess, I. V. Moskalenko, and S. S. Ostapchenko, Astrophys. J. **803**, 54 (2015).
- [24] R. Ulrich, R. Engel and M. Unger, Phys. Rev. D **83**, 054026 (2011).
- [25] R. Engel, D. Heck, and T. Pierog, Annu. Rev. Nucl. Part. Sci. **61**, 467 (2011).
- [26] O. Adriani *et al.* (LHCf Collaboration), Phys. Rev. D **94**, 032007 (2016).
- [27] S. Chatrchyan *et al.* (CMS and TOTEM Collaborations), Eur. Phys. J. C **74**, 3053 (2014);
G. Antchev *et al.* (TOTEM Collaboration), *ibid.* **75**, 126 (2015).
- [28] J. Bjorken, S. Brodsky, and H. J. Lu, Phys. Lett. B **286**, 153 (1992).
- [29] G. Aad *et al.* (ATLAS Collaboration), Eur. Phys. J. C **72**, 1926 (2012).
- [30] V. A. Khoze, F. Krauss, A. D. Martin, M. G. Ryskin, and K. C. Zapp, Eur. Phys. J. C **69**,
85 (2010).

- [31] E.-J. Ahn, R. Engel, T. K. Gaisser, P. Lipari, and T. Stanev, Phys. Rev. D **80**, 094003 (2009).
- [32] P. Skands, S. Carrazza, and J. Rojo, Eur. Phys. J. C **74**, 3024 (2014).
- [33] CMS Collaboration, Reports No. CMS-PAS-FSQ-16-002 and No. CMS-PAS-FSQ-15-006.
- [34] R. D. Ball *et al.*, Nucl. Phys. **B877**, 290 (2013).